Improving the use of the randomized singular value decomposition for the inversion of gravity and magnetic data

Saeed Vatankhah¹, Shuang Liu², Rosemary Anne Renaut³, Xiangyun Hu², and Jamaledin Baniamerian4

ABSTRACT

The focusing inversion of gravity and magnetic potentialfield data using the randomized singular value decomposition (RSVD) method is considered. This approach facilitates tackling the computational challenge that arises in the solution of the inversion problem that uses the standard and accurate approximation of the integral equation kernel. We have developed a comprehensive comparison of the developed methodology for the inversion of magnetic and gravity data. The results verify that there is an important difference between the application of the methodology for gravity and magnetic inversion problems. Specifically, RSVD is dependent on the generation of a rank q approximation to the underlying model matrix, and the results demonstrate that q needs to be larger, for equivalent problem sizes, for the magnetic problem compared to the gravity problem. Without a relatively large q, the dominant singular values of the magnetic model matrix are not well approximated. We determine that this is due to the spectral properties of the matrix. The comparison also shows us how the use of the power iteration embedded within the randomized algorithm improves the quality of the resulting dominant subspace approximation, especially in magnetic inversion, yielding acceptable approximations for smaller choices of q. Further, we evaluate how the differences in spectral properties of the magnetic and gravity input matrices also affect the values that are automatically estimated for the regularization parameter. The algorithm is applied and verified for the inversion of magnetic data obtained over a portion of the Wuskwatim Lake region in Manitoba, Canada.

INTRODUCTION

Potential-field surveys, gravity and magnetic, have been used for many years for a wide range of studies including oil and gas exploration, mining applications, and mapping basement topography (Blakely, 1996; Nabighian et al., 2005). The inversion of acquired data is one of the important steps in the interpretation process (Pilkington, 1997; Li and Oldenburg, 1998; Portniaguine and Zhdanov, 1999; Boulanger and Chouteau, 2001; Silva and Barbosa, 2006; Farguharson, 2008; Liu et al., 2013, 2018). The problem is, however, ill posed, and the solution process requires the minimization of a global objective function that consists of two terms, the data misfit term and a stabilizing or regularizing term. These two terms are balanced by a scalar regularization parameter that weights the contribution of the stabilizing term to the solution. Extensive background on the modeling and solution techniques is provided in the literature (Li and Oldenburg, 1998; Portniaguine and Zhdanov, 1999; Vatankhah et al., 2015). Still, the development of effective and efficient approaches for large-scale problems continues to be computationally challenging, and many directions for reducing this burden have been considered. Among these, for example, one focus has been on reducing the computational demands, whether memory or floating-point

Manuscript received by the Editor 8 September 2019; revised manuscript received 15 May 2020; published ahead of production 14 June 2020; published online 17 August 2020.

China University of Geosciences, Institute of Geophysics and Geomatics, Hubei Subsurface Multi-scale Imaging Key Laboratory, Wuhan 430074, China and University of Tehran, Institute of Geophysics, Tehran 14359-44411, Iran. E-mail: svatan@ut.ac.ir.

China University of Geosciences, Institute of Geophysics and Geomatics, Hubei Subsurface Multi-scale Imaging Key Laboratory, Wuhan 430074, China. E-mail: lius@cug.edu.cn (corresponding author); xyhu@cug.edu.cn.

³Arizona State University, School of Mathematical and Statistical Sciences, Tempe, Arizona 85287-1804, USA. E-mail: renaut@asu.edu.

⁴Graduate University of Ádvanced Technology, Department of Earth Sciences, College of Sciences and Modern Technologies, Kerman 7631818356, Iran and University of Roma Tre, Department of Mathematics and Physics, Rome 84-00146, Italy. E-mail: jamaledin.baniamerian@gmail.com. © 2020 Society of Exploration Geophysicists. All rights reserved.

G94 Vatankhah et al.

operations, using compression techniques as in Portniaguine and Zhdanov (2002), Li and Oldenburg (2003), and Cox et al. (2010), or on techniques that implement a restricted systematic search algorithm as described in Uieda and Barbosa (2012). Our research also is directed toward the reduction of the computational burden.

A widely used strategy is to restrict an original large-scale problem to a much smaller subspace (Skilling and Bryan, 1984; Oldenburg et al., 1993). The resulting subspace solution then can be projected back to the original full space under reasonable assumptions that the subspace problem sufficiently captures the characteristics of the full-space problem. For example, using the Golub-Kahan bidiagonalization (GKB) of the model matrix, the large-scale problem is projected onto a Krylov subspace of restricted dimension. The subspace solution then is obtained relatively efficiently using a standard factorization such as singular value decomposition (SVD) (Paige and Saunders, 1982a, 1982b; Kilmer and O'Leary, 2001; Chung et al., 2008; Renaut et al., 2017; Vatankhah et al., 2017). We note that this approach is equivalent to the use of the conjugate gradient (CG) algorithm for the solution of the least-squares problem in exact arithmetic, but it is more stable numerically (Paige and Saunders, 1982a). Still, there is a need to solve ever larger problems so as to provide greater resolution of the subsurface structures, while also automatically estimating a suitable regularization parameter. Even with the continually increasing computational power and memory that is available, it is sometimes impossible or computationally prohibitive to obtain effective solutions with these traditional computational algorithms.

Recently, the powerful concept of randomization for finding low-rank approximations has been introduced as an alternative strategy for dealing with large-scale inverse problems (Halko et al., 2011; Xiang and Zou, 2013; Voronin et al., 2015; Xiang and Zou, 2015; Wei et al., 2016; Vatankhah et al., 2018a, 2018b). Fundamentally, for a given matrix, the approach consists of three steps: (1) a stochastic step that generates a random but orthonormal matrix that samples rows and columns of a matrix, (2) a completely deterministic step that yields the eigendecomposition of the subsampled matrix, and (3) the use of the eigendecomposition to provide a low-rank approximate SVD of the matrix. The resulting randomized SVD (RSVD) then is used within an inversion methodology for finding a solution of the underlying large-scale problem.

For the 3D inversion of gravity data, Vatankhah et al. (2018b) combine an L_1 -norm regularization strategy with the RSVD for the generation of a focused image of the subsurface with n model parameters using just m data measurements, $m \ll n$. For the RSVD algorithm, it is important to estimate an appropriate lower bound on q in order that acceptable solutions are provided using an algorithm that is computationally efficient with respect to time and memory. Their results indicate that satisfactory results, nearly equivalent to those using the full SVD (FSVD) for the SVD calculations in the algorithm, are achievable using a rank q approximation $q \gtrsim (m/6)$. (The solutions are the same when q = m.) Note that throughout we will use RSVD and FSVD to denote the algorithms that use the RSVD and FSVD, respectively, to approximate the SVD of the sensitivity matrices at all steps in the L_1 -norm regularization strategy.

The main contribution of this paper is the extension of the RSVD algorithm, as presented in Vatankhah et al. (2018b), for the inversion of magnetic potential data. First, our results demonstrate that direct application of their RSVD algorithm does not lead to acceptable solutions. Rather, for a problem of equivalent size as given by

the pair (m, n), we find that q must be larger than predicted for the gravity problem; here, the choice q < m/2 does not yield acceptable solutions. But, increasing q significantly is contrary to the aim of finding an algorithm that is effective and memory limited; as q increases, there is no benefit in memory reduction by using RSVD in place of FSVD. Here, we show that the difference between the gravity and magnetic problems is due to the spectral properties of the underlying sensitivity matrices. For the magnetic problem, the spectral values decrease more slowly; hence, a larger q is required to accurately capture the essential properties of the original problem to the same degree of accuracy as for the gravity problem. However, by introducing power iterations into the determination of the rank-q approximation, an improved approximation of the spectrum is achieved and the rank q approximation error decreases. Then, with just one power iteration for each sensitivity matrix, acceptable results are achieved for $q \ge m/4$. Moreover, introducing the same power iteration for the gravity problem reduces the acceptable rank to $q \gtrsim m/8$. Our analysis of the spectrum also shows that the regularization parameter(s) required in the solves for the magnetic problem are commensurately larger due to the larger dominant spectral values of its model matrix compared to the gravity problem. In both cases, however, we demonstrate that given the suitable RSVD algorithm, it still is possible to automatically estimate the suitable, and problem-dependent, regularization parameter using standard techniques. Hence, this work extends and validates the use of the L_1 norm stabilization algorithm combined with the RSVD for inversion of gravity and magnetic data sets.

INVERSION METHODOLOGY

We discuss the general case for the linear inversion of potential-field data in which the subsurface is discretized into a large number of cells of fixed size but with unknown physical properties (Li and Oldenburg, 1998; Boulanger and Chouteau, 2001). The unknown parameters of the cells are stacked in a real vector of length n, $\mathbf{m} \in \mathcal{R}^n$, potential-field data measured at m stations $m \ll n$ are stacked in a vector $\mathbf{d}_{\text{obs}} \in \mathcal{R}^m$, and the measurements are connected to the model parameters via the model matrix $\mathbf{G} \in \mathcal{R}^{m \times n}$, yielding the underdetermined linear system

$$\mathbf{d}_{\text{obs}} = \mathbf{Gm}.\tag{1}$$

Matrix G is the forward model operator that maps from model to data spaces, with entry G_{ij} representing the effect of the unit model parameter at cell j on the data at location i. In the case of the inversion of magnetic data, vector m represents the values of the unknown susceptibilities of the cells and \mathbf{d}_{obs} is the total magnetic field. Rao and Babu (1991) provide a fast approach for computing the total magnetic field anomaly of a cube that is used to form the elements of G for the magnetic problem. For the gravity problem, the vectors \mathbf{m} and \mathbf{d}_{obs} are the cell density contrasts and vertical components of the gravity field, respectively. Here, the elements of G are computed using the formula developed by Haáz (1953); see, for example, Boulanger and Chouteau (2001) for more details. Clearly, model matrix G depends on the kernels that connect the data and measurements. Thus, we may anticipate that the properties of G are problem-dependent. In particular, the spectral properties of G affect the condition of the underdetermined system and, hence, the performance of any algorithm that is used for data inversion.

Stabilization, or regularization, is required to find an acceptable solution of the ill-posed system given by equation 1; its solution is neither unique nor stable. Here, we consider the L_1 -norm-stabilized solution of equation 1, as presented by Vatankhah et al. (2017), to reconstruct high-resolution sharp images of the subsurface. Although such L_1 -norm algorithms have been developed in many contexts (see the references in Vatankhah et al. [2017]), their application for the focusing inversion of geophysical structures as presented in Vatankhah et al. (2017) appears to be novel. In particular, their approach included (1) weighting of the data based on the knowledge, or estimate, of the standard deviation of the independent noise in the data, encoded in diagonal matrix W_d , (2) weighting for the depths of the cells encoded in $\mathbf{W}_{\text{depth}}$ which is a depthweighting matrix with diagonal entries $z^{-\beta}$ at depth z, (3) hard constraints on acceptable values for \mathbf{m} encoded in diagonal matrix \mathbf{W}_{hard} , (4) approximation of the L_1 -norm stabilizer via an L_2 -norm term encoded in W_{L_1} (e.g., Vatankhah et al., 2020, equation 4 with p = 1), and (5) the inclusion of prior knowledge on the solution encoded in \mathbf{m}_{apr} . An estimate for \mathbf{m}_{apr} may come from geology, logging, or previous geophysical surveys or is assumed to be zero when no prior information is available (Li and Oldenburg, 1998). The known values of the model parameters are given in \mathbf{m}_{apr} , and the corresponding elements in W_{hard} are set to a large value. Where there is no information available, the corresponding entries of \mathbf{W}_{hard} and \mathbf{m}_{apr} are set to 1 and 0, respectively. Further details of the application of the hard constraint matrix are provided in Vatankhah et al. (2018b). Overall, solution **m** is estimated as the minimum of the nonlinear global objective function $P^{\alpha}(\mathbf{m})$,

$$\begin{split} \mathbf{m} &= \arg\min_{\mathbf{m}} \{P^{\alpha}(\mathbf{m})\} \\ &= \arg\min_{\mathbf{m}} \{\|\mathbf{W}_{\mathbf{d}}(\mathbf{G}\mathbf{m} - \mathbf{d}_{\text{obs}})\|_{2}^{2} + \alpha^{2} \|\mathbf{W}(\mathbf{m} - \mathbf{m}_{\text{apr}})\|_{2}^{2} \}. \end{split}$$
 (2)

Here, α is a scalar regularization parameter that balances the two terms in the objective function and $W=W_{\text{depth}}W_{\text{hard}}W_{L_1}$ is a product of diagonal invertible matrices (Vatankhah et al., 2020). It is W_{L_1} , which enables the algorithm to produce a nonsmooth and focused image of the subsurface.

Noting that the inverse of a diagonal matrix is obtained at effectively zero computational cost, the objective function expressed in equation 2 easily is transformed to the standard Tikhonov form (Vatankhah et al. [2015]),

$$P^{\alpha}(\mathbf{h}) = \|\tilde{\tilde{\mathbf{G}}}\mathbf{h} - \tilde{\mathbf{r}}\|_{2}^{2} + \alpha^{2}\|\mathbf{h}\|_{2}^{2}, \tag{3}$$

where $\tilde{\tilde{\mathbf{G}}} = \mathbf{W_d}\mathbf{G}\mathbf{W}^{-1}$, $\tilde{\mathbf{r}} = \mathbf{W_d}(\mathbf{d}_{\text{obs}} - \mathbf{G}\mathbf{m}_{\text{apr}})$, and $\mathbf{h} = \mathbf{W}(\mathbf{m} - \mathbf{m}_{\text{apr}})$. The solution of equation 3, dependent on the choice of α , then is

$$\mathbf{h}(\alpha) = (\tilde{\tilde{\mathbf{G}}}^T \tilde{\tilde{\mathbf{G}}} + \alpha^2 \mathbf{I}_n)^{-1} \tilde{\tilde{\mathbf{G}}}^T \tilde{\mathbf{r}}, \tag{4}$$

and the model update is given by

$$\mathbf{m}(\alpha) = \mathbf{m}_{\text{apr}} + \mathbf{W}^{-1}\mathbf{h}(\alpha). \tag{5}$$

The nonlinear objective function is minimized using an iteratively reweighted approach, yielding $\mathbf{m}(\alpha)$, dependent not only on α ,

changing with each iteration, but also on matrix W, which changes at each step through the update of matrix W_{L_1} . Further, it is well known that it is important to apply suitable bound constraints within a focusing inversion of magnetic or gravity data, e.g., Portniaguine and Zhdanov (1999). At each stage of the algorithm, upper and lower bounds on the physical parameters are imposed in order that the recovered model is reliable and within known acceptable ranges. If at any iteration a physical parameter value falls outside these predefined lower and upper bounds, the value is projected back to the nearest upper or lower bound (Boulanger and Chouteau, 2001). The iteration is terminated when either the data predicted by the reconstructed model satisfies the observed data at the noise level or a maximum number of iterations K_{max} is reached. The complete algorithm is described in Vatankhah et al. (2017).

When m and n are small, it is feasible to express the solution $\mathbf{h}(\alpha)$ using the full SVD of $\tilde{\mathbf{G}}$. For $\tilde{\mathbf{G}} = \mathbf{U}\Sigma\mathbf{V}^T$, where matrices $\mathbf{U} \in \mathcal{R}^{m \times m}$ and $\mathbf{V} \in \mathcal{R}^{n \times n}$ are orthogonal with columns \mathbf{u}_i and \mathbf{v}_i and \mathbf{v}_i and \mathbf{v}_i is the matrix of singular values σ_i , ordered from large to small, then

$$\mathbf{h}(\alpha) = \sum_{i=1}^{m^*} \frac{\sigma_i^2}{\sigma_i^2 + \alpha^2} \frac{\mathbf{u}_i^T \tilde{\mathbf{r}}}{\sigma_i} \mathbf{v}_i$$
 (6)

see, e.g., Paoletti et al. (2014), Vatankhah et al. (2015), and Vatankhah et al. (2017). Here, m^* , the number of nonzero singular values, is the numerical rank of the matrix, namely, $m^* \le m$. It also is relevant that it is the availability of the FSVD that makes it possible to estimate regularization parameter α cheaply using standard parameter-choice techniques without calculating the solution of the problem multiple times (Xiang and Zou, 2013; Chung and Palmer, 2015). Unfortunately, calculation of SVD for large, or even moderate, underdetermined systems is not practical; the cost is approximately $6nm^2 + 20m^3$ (Golub and Van Loan, 2013). A traditional alternative is the use of the iterative GKB algorithm that can be used to project G onto a Krylov subspace of smaller dimension, theoretically equivalent to the use of CG on the least-squares system, and for which an SVD of the projected problem then is efficiently used to yield the subspace solution; see Vatankhah et al. (2017) for details of the application of this strategy to find the minimizer of $P^{\alpha}(\mathbf{h})$. Although the SVD obtained via the GKB algorithm facilitates the use of SVD-based parameter-choice algorithms to find an optimal α at minimal additional computational cost, and the solution is projected back to the original full space at minimal cost, the GKB algorithm relies on building a relatively large Krylov space for the solution when m and n are large; see e.g., Renaut et al. (2017) and Vatankhah et al. (2017). Generating the Krylov space is computationally relatively expensive and thus restricts the set of problems that can be considered. The use of the Krylov space to find solution $\mathbf{m}(\alpha)$ as given by equation 5 for a fixed α , specifically when α is assumed known and not adjusted to fit the problem, is commonly known as the CG least-squares method. It is thus similarly limited computationally, as discussed in Renaut et al. (2017). Here we focus, therefore, on the efficient estimate of an approximate SVD using randomization. We note that an extensive comparison of the application of the GKB and RSVD algorithms for minimizing $P^{\alpha}(\mathbf{h})$ for the gravity inverse problem is considered in Vatankhah et al. (2018b). We refer to this reference for the Vatankhah et al.

comparison of the operation costs and the details of the numerical implementation.

Regularization parameter-choice method

G96

Given an estimate for the SVD of $\tilde{\mathbf{G}}$, we can make use of parameter-choice rules to find an optimal choice for α , which we denote as α_{opt} , but note that it is optimal only in the sense of the chosen method. Here, we use the method of unbiased predictive risk estimation (UPRE) to find α_{opt} . This a posteriori rule for choosing the Tikhonov regularization parameter is well-described in Vogel (2002) and has been extensively applied for the inversion of data when an estimate of the noise covariance is available, including for the inversion of geophysical data (Vatankhah et al., 2015, 2017) and for more general inversion problems (Chung and Palmer, 2015; Renaut et al., 2017). Using the FSVD of matrix $\tilde{\mathbf{G}}$, the UPRE function to be minimized is given by

$$U(\alpha) = \sum_{i=1}^{m^*} \left(\frac{1}{\sigma_i^2 \alpha^{-2} + 1}\right)^2 (\mathbf{u}_i^T \tilde{\mathbf{r}})^2 + 2\left(\sum_{i=1}^{m^*} \frac{\sigma_i^2}{\sigma_i^2 + \alpha^2}\right) - m^*.$$
(7)

Parameter $\alpha_{\rm opt}$ is found by evaluating this equation on a range of α , between minimum and maximum σ_i . In keeping with standard approaches, this approach is used to find $\alpha_{\rm opt}^{(k)}$ for iterations k > 1, but for k = 1

$$\alpha^{(1)} = \left(\frac{n}{m}\right)^{3.5} \frac{\sigma_1}{\text{mean}(\sigma_i)} \tag{8}$$

is used. This follows Vatankhah et al. (2017) and is based on the suggestion of Farquharson and Oldenburg (2004), in which it is recommended that a large α should always be applied at the first iteration.

Randomized SVD

Recent approaches based on randomization have presented an interesting alternative for tackling problems requiring high resolution of the subsurface (Xiang and Zou, 2013; Voronin et al., 2015; Vatankhah et al., 2018a, 2018b). Random sampling is used to construct a low-dimensional subspace that approximates the column space of the model matrix and maintains the most dominant spectrum of the original matrix (Halko et al., 2011). Standard deterministic matrix decomposition methods such as the SVD, or eigendecomposition, then can be used to compute a low-rank approximation of the original matrix. Specifically, in the context of potential-field inversion, it is desirable to find a q-rank matrix $\tilde{\tilde{\mathbf{G}}}_a$, which is as close as possible to $\tilde{\tilde{\mathbf{G}}}$ in the least-squares sense, whereas at the same time, the target rank q is as small as possible in order that the inversion process is fast. We note that, of course, the best rank q approximation in the least-squares sense is given by the exact truncated SVD of $\tilde{\mathbf{G}}$ with q terms (Golub and Van Loan, 2013). It is generally, however, not practical to calculate the truncated SVD for large-scale problems. Thus, here we focus on the RSVD and carefully describe the approach that was presented in Vatankhah et al (2018b) for the solution of the gravity inversion problem.

The fundamental aspects of an RSVD algorithm consist of three stages. Here, we present this for the underdetermined matrix $\tilde{\mathbf{G}}$. (1) A low-dimensional subspace is constructed that approximates the column space of $\tilde{\tilde{\mathbf{G}}}^T$. The aim is to find a matrix $\mathbf{Q} \in \mathcal{R}^{n \times q}$ with orthonormal columns such that $\tilde{\tilde{\mathbf{G}}} \approx \tilde{\tilde{\mathbf{G}}} \mathbf{Q} \mathbf{Q}^T$. (2) Given the near-optimal basis spanned by the columns of Q, a smaller matrix $\mathbf{B} = \tilde{\mathbf{G}}\mathbf{Q} \in \mathcal{R}^{m \times q}$ is formed. This means that $\tilde{\mathbf{G}}$ is restricted to the smaller subspace spanned by the basis from the columns of Q and its Euclidean norm is preserved (Erichson et al., 2016). (3) **B** can be used to compute an approximate SVD for $\tilde{\mathbf{G}}$ using a traditional algorithm to compute the approximations to the first q left singular vectors as well as the corresponding singular values for matrix $\tilde{\mathbf{G}}$. The approximate right singular vectors also could be recovered; see e.g., Xiang and Zou (2013). Alternatively, as discussed, with proof, in Vatankhah et al. (2018b), the much smaller matrix $\mathbf{B}^T \mathbf{B} \in \mathcal{R}^{\ell \times \ell}$ can be used to find the required SVD components for **B** using the eigendecomposition of $\mathbf{B}^T \mathbf{B}$. Here, $\ell = q + p$, where p is a small oversampling parameter. It also was demonstrated that the computational cost of this algorithm is $O(\ell mn)$. Thus, it is feasible to compute the large singular values of a given matrix efficiently. Note that although step (1) is completely random and depends on the selection of a specific approach to find Q, steps (2) and (3) are deterministic.

The fundamental approach, as presented by Vatankhah et al. (2018b), is summarized in Algorithm 1. A power iteration can be included at step 3 of this algorithm to improve the quality of the approximate SVD. This is needed when the spectrum does not decay quickly. The power iteration algorithm is explained in the following section.

Randomized SVD with power iterations

The quality of the RSVD that is obtained using Algorithm 1 without step 3 depends on the quality of the basis matrix \mathbf{Q} as providing a basis for the column space of $\tilde{\mathbf{G}}^T$. Halko et al. (2011) suggest an

Algorithm 1. RSVD algorithm with s power iterations. Given matrix $\tilde{\tilde{G}} \in \mathcal{R}^{m \times n} (m < n)$, a target matrix rank q and a small constant oversampling parameter p satisfying $q + p = \ell \ll m$, compute an approximate SVD of $\tilde{\tilde{G}} : \tilde{\tilde{G}} \approx U_q \Sigma_q V_q^T$ with $U_q \in \mathcal{R}^{m \times q}, \Sigma_q \in \mathcal{R}^{q \times q}, V_q \in \mathcal{R}^{n \times q}$.

- 1: Generate $\Omega \in \mathcal{R}^{\ell \times m}$, where all entries are drawn from a standard normal distribution: $\Omega = \operatorname{randn}(\ell, m)$.
- 2: Form the sketch matrix $\mathbf{Y} = \Omega \tilde{\mathbf{G}} \in \mathcal{R}^{\ell \times n}$.
- 3: When $s \ge 1$: apply power iterations; see Algorithm 2.
- 4: Compute orthonormal matrix $\mathbf{Q} \in \mathcal{R}^{n \times \ell}$ via QR factorization $\mathbf{Y}^T = \mathbf{Q}\mathbf{R}$.
- 5: Form the matrix $\mathbf{B} = \tilde{\mathbf{G}}\mathbf{Q} \in \mathcal{R}^{m \times \ell}$.
- 6: Compute the matrix $\mathbf{B}^T \mathbf{B} \in \mathcal{R}^{\ell \times \ell}$.
- 7: Compute the eigendecomposition of $\mathbf{B}^T \mathbf{B}$; $[\tilde{\mathbf{V}}_{\ell}, \mathbf{D}_{\ell}] = \text{eig}(\mathbf{B}^T \mathbf{B})$.
- 8: Compute $\mathbf{V}_q = \mathbf{Q} \tilde{\mathbf{V}}_\ell(:,1\!:\!q); \ \Sigma_q = \sqrt{\mathbf{D}_\ell}(1\!:\!q,1\!:\!q);$ and $\mathbf{U}_{\underline{q}} = \mathbf{B} \tilde{\mathbf{V}}_q(:,1\!:\!q) \ \Sigma_q^{-1}.$
- 9: Note $\tilde{\mathbf{G}}_q = \mathbf{U}_q \mathbf{\Sigma}_q \mathbf{V}_q^T$ is a q-rank approximation of matrix $\tilde{\mathbf{G}}$.

improvement of their proto algorithm for forming the basis matrix \mathbf{Q} and the associated RSVD that should lead to an improved approximation of the dominant spectrum. In the proto algorithm for power iterations (Halko et al., 2011, p. 227), the sketch matrix

 \mathbf{Y} is obtained after first preprocessing matrix $\tilde{\mathbf{G}}$ to give

$$\tilde{\tilde{\mathbf{G}}}^{(s)} = \tilde{\tilde{\mathbf{G}}}(\tilde{\tilde{\mathbf{G}}}^T \tilde{\tilde{\mathbf{G}}})^s, \tag{9}$$

where integer s specifies the number of power iterations. Although this is specifically implemented in Halko et al. (2011), the approach is sensitive to floating-point rounding errors, which reduces the quality of the Q basis. Thus, Halko et al. (2011) implement orthonormalization of the columns of \mathbf{Y} between each application of $\tilde{\mathbf{G}}$ and $\tilde{\mathbf{G}}^T$. Here, we extend the power iterations for the underdetermined case, using Algorithm 2, for step 3 within Algorithm 1, and with complete orthonormalization for the columns of Y. For this step, we use the **QR** factorization of Y^T using an economic **QR** factorization. This means that we generate only the first ℓ columns of the matrix \mathbf{Q} , rather than all n columns that would be obtained using a full $\mathbf{Q}\mathbf{R}$ factorization. Moreover, the matrix \mathbf{R} is not needed and, thus, we use the MATLAB function QR with R not required as an output. This is achieved using $[\mathbf{Q}, \sim] = qr(\mathbf{Y}^T, 0)$, where \sim indicates that **R** is not required (https://www.mathworks .com/help/matlab/ref/gr.html). Furthermore, matrix **Q** is overwritten when proceeding from steps 2 to 3.

To analyze the effect of power iterations on improving the accuracy of the computed matrix, a simplified upper bound on the expected error between the original and the *q*-rank-computed matrices is given by Martinsson (2016) and Erichson et al. (2016)

$$\begin{split} E \| \tilde{\tilde{\mathbf{G}}} - \tilde{\tilde{\mathbf{G}}} q \| &\leq [1 + \sqrt{\frac{q}{p-1}} \\ &+ \frac{e\sqrt{q+p}}{p} . \sqrt{\min(m,n) - q}]^{\frac{1}{2s+1}} \sigma_{q+1}, \end{split} \tag{10}$$

where e is Euler's number, σ_{q+1} is the q+1 largest singular value of matrix $\tilde{\mathbf{G}}$, E denotes the expectation operator, and it is assumed that $p \geq 2$. The upper bound (9) indicates how parameters p,q, and s can be used to control the approximation error. Note immediately that for $q = \min(m,n)$ then $\sigma_{q+1} = 0$ and $E \| \tilde{\mathbf{G}} - \tilde{\mathbf{G}}_q \| = 0$. With increased oversampling p, the second and third terms in the bracket tend toward zero, which means that the bound approaches the

Algorithm 2. Power iterations. For the given matrix $\tilde{G} \in \mathcal{R}^{m \times n} (m < n)$ and initial sketch matrix $Y \in \mathcal{R}^{\ell \times n}$, improve matrix Y by applying s power iterations.

- 1: For $j = 1, \dots, s$.
- 2: $[\mathbf{Q}, \sim] = qr(\mathbf{Y}^T, 0)$ (economic QR decomposition).
- 3: $[\mathbf{Q}, \sim] = qr(\tilde{\mathbf{G}}\mathbf{Q}, 0)$.
- 4: $\mathbf{Y}^T = \tilde{\mathbf{G}}^T \mathbf{Q}$.
- 5: End.

theoretically optimum value σ_{q+1} (Erichson et al., 2016). As the number of power iterations s increases, 1/(2s+1) goes to zero, and the error bound is reduced.

SYNTHETIC EXAMPLES

In the following, we first evaluate the performance of the RSVD algorithm without power iterations, comparing its performance for the solution of relatively small-scale gravity and magnetic problems under the same configuration but the appropriate choice of model matrix $\tilde{\mathbf{G}}$. The results are compared to those obtained using the FSVD in each case. To understand the performance of the algorithm, we examine the spectrum of the approximate operator, as compared to that of $\tilde{\mathbf{G}}$, for each problem, and then we examine the improvement obtained using the power iterations for s=1. A more complicated configuration for a structure with multiple bodies is then examined, which confirms the conclusions obtained for the first example. First, we provide a discussion of the practical considerations that apply to all of the presented results.

Practical procedures

In the simulations of the total field anomaly, the intensity of the geomagnetic field, the inclination, and the declination are selected as 47 000 nT, 50°, and 2°, respectively. The density contrast and the susceptibilities of the model structures embedded in a homogeneous nonsusceptible background are $\rho = 1 \, \mathrm{gcm}^{-3}$ and $\kappa = 0.1$ (SI unit), respectively. We apply bound constraints at each iteration of the inversion; specifically, $0 = \rho_{\min} \le \rho \le \rho_{\max} = 1$ in units g cm⁻³ and $0 = \kappa_{min} \le \kappa \le \kappa_{max} = 0.1$ in SI units for the gravity and magnetic inversions, respectively. Further, for all simulations, as is standard in the geophysics literature, e.g., Li and Oldenburg (1996) and Leliévre and Oldenburg (2006), we add Gaussian noise with zero mean and standard deviation $(\tau_1 |\mathbf{d}_{\text{exact}}|_i + \tau_2 \max |\mathbf{d}_{\text{exact}}|)$ to datum i, for chosen pairs (τ_1, τ_2) , where $\mathbf{d}_{\text{exact}}$ is the exact data set, yielding $\mathbf{d}_{\mathrm{obs}}$ with a known distribution of noise for the error. This standard deviation is used to generate the matrix W_d in the data fit term. The values of (τ_1, τ_2) are selected such that the signal-to-noise ratios (S/Ns), as given by

$$S/N = 20 \log_{10} \frac{\|\mathbf{d}_{\text{exact}}\|_2}{\|\mathbf{d}_{\text{obs}} - \mathbf{d}_{\text{exact}}\|_2},$$
 (11)

are close for the gravity and magnetic noise-contaminated data. The values for (τ_1, τ_2) and the resulting S/Ns are specified in the captions of figures associated with the results for each data set. Then, to test convergence of the update $\mathbf{m}^{(k)}$ at iteration k, we calculate the χ^2 estimate,

$$(\chi^2)^{(k)} = \|\mathbf{W_d}(\mathbf{d_{obs}} - \mathbf{d_{pre}^{(k)}})\|_2^2,$$
 (12)

where $\mathbf{d}_{\mathrm{pre}}^{(k)} = \mathbf{G}\mathbf{m}^{(k)}$, and that assesses the predictive capability of the current solution. When $(\chi^2)^{(k)} \leq m + \sqrt{2m}$, the iteration terminates. Otherwise, the iteration is allowed to proceed in all cases to a maximum number of iterations $K_{\mathrm{max}} = 50$. In all simulations, as suggested in Vatankhah et al. (2018a), we use a fixed oversampling parameter p = 10, which determines $\ell = q + 10$. We also assume $\mathbf{m}_{\mathrm{apr}} = \mathbf{0}$, and for $\mathbf{W}_{\mathrm{depth}}$, take $\beta = 0.8$ and 1.4, for gravity and magnetic inversions, respectively, which are values close to those

G98 Vatankhah et al.

suggested by Li and Oldenburg (1998). In the results, we examine the dependence of the solution on the choice of q and record (1) the number of iterations K required, (2) the relative error progression with increasing k as given by

$$RE^{(k)} = \frac{\|\mathbf{m}_{\text{exact}} - \mathbf{m}^{(k)}\|_{2}}{\|\mathbf{m}_{\text{exact}}\|_{2}},$$
 (13)

(3) the relative error in the rank q approximation to $\tilde{\tilde{\mathbf{G}}}$,

a)
$$0 = 0.00$$
 0.00 0.00 0.00 0.00 0.00 0.00 0.00 0.00 0.00 0.00 Easting (m)

Figure 1. Cross section of the synthetic model consisting of two dipping dikes. (a) Density distribution and (b) susceptibility distribution.

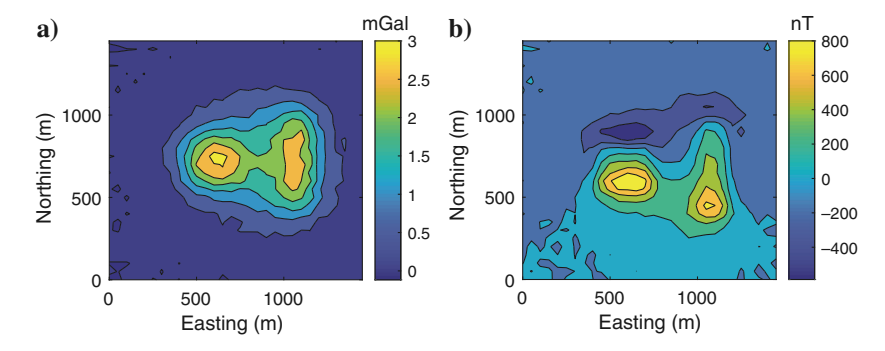


Figure 2. Anomaly produced by the model shown in Figure 1 and contaminated by Gaussian noise. (a) Vertical components of the gravity field. The noise is generated using parameter pairs ($\tau_1 = 0.02, \tau_2 = 0.02$) and (b) total magnetic field. Here, ($\tau_1 = 0.02, \tau_2 = 0.015$). The S/Ns for the gravity and magnetic data, respectively, are 21.9188 and 21.7765.

$$\mathbf{RG}^{(k)} = \frac{\|\tilde{\tilde{\mathbf{G}}} - \tilde{\tilde{\mathbf{G}}}_q^{(k)}\|_2}{\|\tilde{\tilde{\mathbf{G}}}\|_2},\tag{14}$$

(4) $\alpha^{(k)}$ with increasing k, and (5) all values at the final iteration K as well as the time for the iterations. Moreover, in all cases, we do not include the calculation of the original model matrix G.

In the subsequent discussion of the simulations, we present results for gravity and magnetic data inversions. To carefully contrast how the two models differ, we present in each case first results using the gravity data, and then the equivalent problem but inverted for magnetic data. Our aim is not to show that the algorithm can suc-

ceed for gravity data inversion because that has already been demonstrated in the literature, but to emphasize the impact of changing the model to the magnetic data case, for which the sensitivity matrix presents with different spectral properties. Computations are performed on a desktop computer with an Intel Xeon W-2133 CPU 3.6 GHz processor and 32 GB RAM.

Small-scale model consisting of two dipping dikes

The small-scale but complicated structure of two dipping dikes, illustrated in Figure 1, makes it computationally feasible to compare the solutions for the gravity and magnetic inverse problems using Algorithm 1 without power iteration, with the solutions obtained using FSVD. The data for the problem are generated on the surface on a $30 \times 30 = 900$ grid with grid spacing 50 m. The noisy gravity and magnetic data are illustrated in Figure 2a and 2b.

The subsurface volume is discretized into $900 \times 10 = 9000$ cubes of size 50 m in each dimension, for a model extending to depth 500 m. The resulting matrix $\tilde{\mathbf{G}}$ is small, of size 900×9000 , and it is computationally feasible to calculate the FSVD of $\tilde{\mathbf{G}}$. This facilitates the comparison of solutions obtained with the inversion algorithm using the FSVD and an approximate SVD obtained using the RSVD. Results obtained using the FSVD and RSVD, with the

Table 1. Results of the inversion algorithms applied on the gravity data of Figure 2a.

Method	q	$lpha^{(1)}$	$lpha^{(K)}$	$RE^{(K)}$	$RG^{(K)}$	K	χ^2	Time (s)
FSVD	_	61,712	32.2	0.7232	_	12	811.8	31.5
RSVD	100	24,074	44.5	0.7550	0.0521	14	935.8	37.2
	150	29,524	37.4	0.7441	0.0497	12	928.7	32.7
	200	33,726	34.5	0.7221	0.0448	12	905.6	32.3
	300	40,360	33.4	0.7153	0.0257	12	901.4	33.0
	500	49,504	29.5	0.7077	0.0143	12	801.9	35.0
	700	56,105	31.1	0.7061	0.0082	12	908.1	35.9
	900	61,712	32.2	0.7232	$2.8510e^{-14}$	12	811.8	37.9

choices $q=100,\,150,\,200,\,300,\,500,\,700,$ and 900, are detailed in Tables 1 and 2, respectively, and are illustrated in Figures 3–6. Specifically, Figures 3 and 5 illustrate the results using the FSVD for the gravity and magnetic data inversions, respectively. For comparison, Figures 4 and 6 illustrate the results using the RSVD with q=200 for the gravity and magnetic data inversions, respectively.

The results presented for the inversion of the gravity data using the FSVD show that the iteration terminates after just 12 iterations, and, as indicated in Figure 3a, the reconstructed model is in good agreement with the original model. A sharp and focused image of the subsurface is obtained, and, although the depths to the top of the structures are consistent with those of the original model, the extensions of the dikes are overestimated for the left dike and underestimated for the right dike. Figure 3b and 3c illustrates the progression of the relative error and regularization parameter at each iteration, respectively. Figure 3d shows the UPRE function at the final iteration. These figures are presented for comparison with the results obtained using the RSVD algorithm and demonstrate that $\alpha^{(k)}$ is much larger for the magnetic problem as compared to the gravity problem of the same size, confirming that it is important to automatically adjust $\alpha^{(k)}$ for the given model and iteration.

For the same gravity problem, the results using the RSVD algorithm for very small values of q, q < 100 are not acceptable. With the increasing q, the solution improves until, at q = m, the solution matches the FSVD solution. For the reported choices of q, all the solutions terminate prior to $K_{\rm max}$, with K = 12 for $q \ge 150$ and demonstrating that the χ^2 estimate is satisfied. We can see that for a suitable value of q, the RSVD leads to a solution that is close to that achieved using the FSVD. These conclusions confirm the results in Vatankhah et al. (2018b); the RSVD algorithm can be used with $q \ge (m/6)$ for the inversion of gravity data. We illustrate the results of the inversion using q = 200 in Figure 4.

The results presented for the inversion of the magnetic data using the FSVD show that the iteration terminates after eight iterations, and, as indicated in Figure 5a, the reconstructed model is in reasonable agreement with the original model. Again, a focused image of the subsurface is obtained, but the overestimation of the depth of the

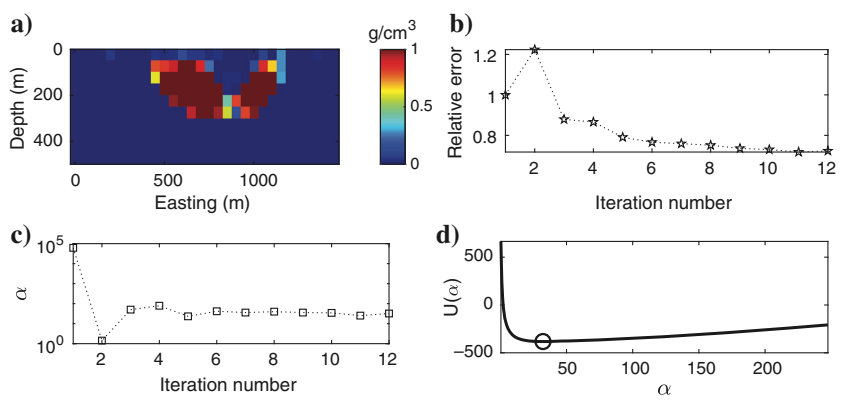


Figure 3. FSVD results for the inversion of gravity data given in Figure 2a. (a) Cross section of reconstructed model, (b) the progression of relative error $RE^{(k)}$ with iteration k, (c) the progression of regularization parameter $\alpha^{(k)}$ with iteration k, and (d) the UPRE function at the final iteration.

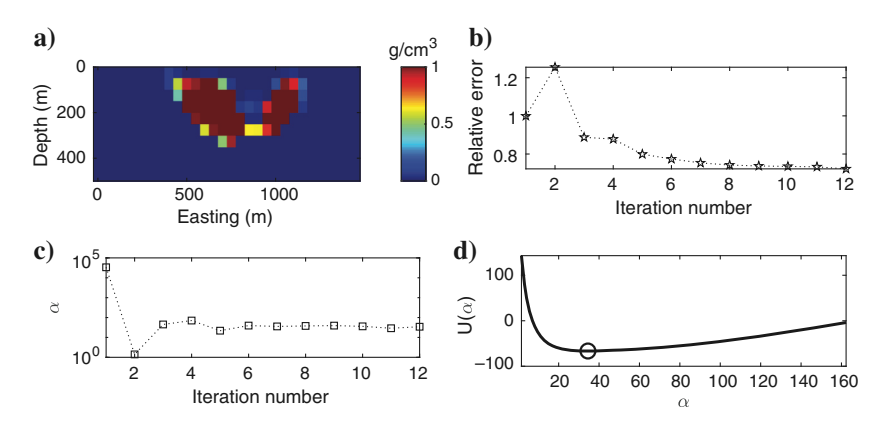


Figure 4. RSVD results using target rank q=200 for the inversion of gravity data given in Figure 2a. (a) Cross section of reconstructed model, (b) the progression of relative error $RE^{(k)}$ with iteration k, (c) the progression of regularization parameter $\alpha^{(k)}$ with iteration k, and (d) the UPRE function at the final iteration.

Table 2. Results of the inversion algorithms applied on the magnetic data of Figure 2b.

Method	q	$a^{(1)}$	$\alpha^{(K)}$	$RE^{(K)}$	$RG^{(K)}$	K	χ^2	Time (s)
FSVD	_	21,086	4106.4	0.8454	_	8	898.6	20.7
RSVD	100	9866	4372.3	1.0651	0.3735	50	2880.6	125.0
	150	11,247	3089.6	0.9904	0.4143	50	2592.5	127.9
	200	12,415	3018.0	0.9050	0.3701	50	1673.7	134.9
	300	14,371	3030.9	0.8606	0.2948	50	1120.5	135.0
	500	17,011	3861.2	0.8426	0.0453	9	917.6	26.9
	700	19,071	3854.1	0.8470	0.0268	8	918.2	24.8
	900	21,086	4106.4	0.8454	$2.8165e^{-14}$	8	898.6	26.1

G100 Vatankhah et al.

left dike is greater compared with the results in Figure 3. Correspondingly, the relative error is larger than that achieved in the inversion of the gravity data. For the same magnetic problem, the

6

Iteration number

a) b) 0 Relative error Depth (m) 200 4 6 Iteration number Easting (m) **d**) ₁₀₀₀ c) 10 500 (♡ ∩ 0

Figure 5. FSVD results for the inversion of magnetic data given in Figure 2b. (a) Cross section of the reconstructed model, (b) the progression of relative error $RE^{(k)}$ with iteration k, (c) the progression of regularization parameter $\alpha^{(k)}$ with iteration k, and (d) the UPRE function at the final iteration.

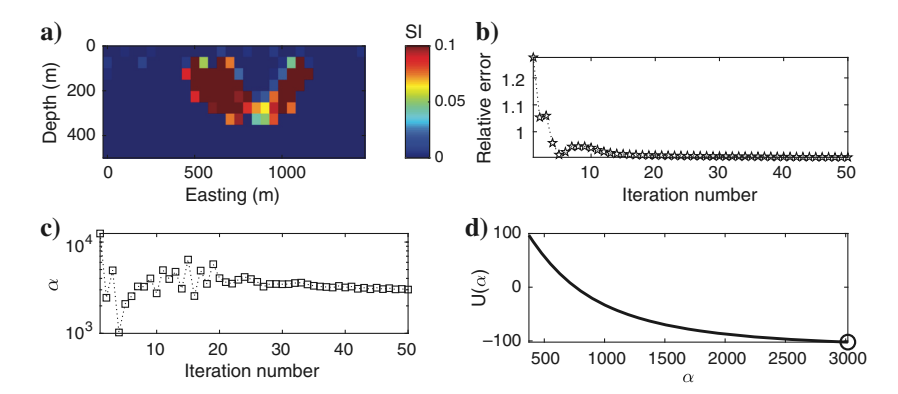


Figure 6. RSVD results using target rank q = 200 for the inversion of magnetic data given in Figure 2b. (a) Cross section of the reconstructed model, (b) the progression of relative error RE^(k) with iteration k, (c) the progression of regularization parameter $\alpha^{(k)}$ with iteration k, and (d) the UPRE function at the final iteration.

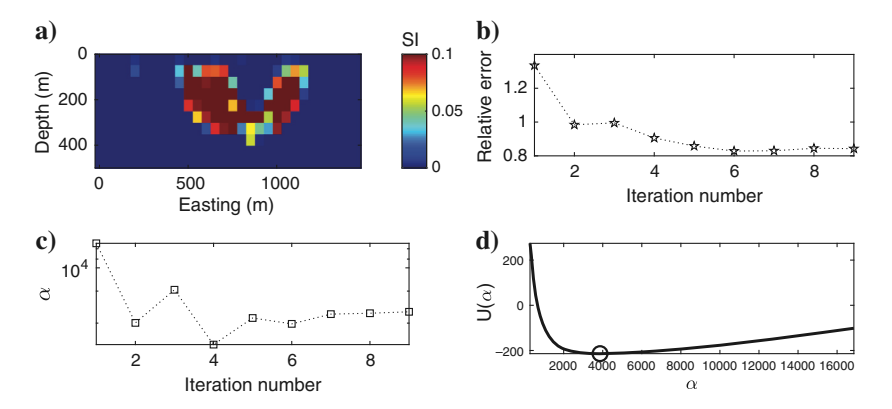


Figure 7. RSVD results using target rank q = 500 for the inversion of magnetic data given in Figure 2b. (a) Cross section of the reconstructed model, (b) the progression of relative error RE^(k) with iteration k, (c) the progression of regularization parameter $\alpha^{(k)}$ with iteration k, and (d) the UPRE function at the final iteration.

results using the RSVD algorithm are not acceptable with reasonable choices for q; indeed, the algorithm does not terminate prior to $K = K_{\text{max}}$ for q < 500, and the cost therefore increases signifi-

cantly. As compared to the inversion of gravity data, larger values of q are required to yield acceptable results. Observe, for example, that q = 200 is not a suitable choice because the relative error of the reconstructed model is unacceptable, and the predicted data do not satisfy the observed data at the given noise level; equation 12 is not satisfied for $k \le 50$. Using q = 500, the relative error of the reconstructed model is reduced, and the inversion terminates at nine iterations with an acceptable χ^2 value. We deduce that for the inversion of the magnetic data, it is necessary to take q larger than we would use for the inversion of the gravity data, as is indicated by the much larger value of the rank-q error, RG^(K) in Tables 1 and 2, respectively. To demonstrate the impact of the choice of q, we show the results of the inversion for q = 200 and q = 500, in Figures 6 and 7, respectively.

Spectral properties

×10⁴

We now compare the singular values $\sigma_i^{(k)}$ and $(\sigma_i^{(k)})_q$ for matrices $\tilde{\mathbf{G}}^{(k)}$ and $\tilde{\mathbf{G}}_q^{(k)}$, respectively, for the gravity and magnetic problems in Figures 8 and 9, respectively. In both figures, we show the values for q=200 and q=500 at iteration k=8. It is immediately evident from these plots that the RSVD algorithm does not capture the dominant spectrum of the original matrix for the magnetic problem as closely as is the case for the gravity problem. This clarifies why the magnetic inversion requires larger values of q in order for the inversion to converge. It also is evident that the singular values of the gravity and magnetic problems decay rather slowly, after an initial fast decay.

Power iterations

Now as discussed, the error estimate given in equation 10 will decrease with increasing s. Having seen that the lack of power iterations leads to lack of convergence for the inversion of the magnetic data unless q is taken relatively large $q \gtrsim m/2$, as compared to just $q \gtrsim m/6$ for the gravity problem, we investigate the power iteration step given by Algorithm 2 to improve the column-space approximation of $\tilde{\mathbf{G}}^T$. We therefore repeat the simulations for the data of the two-dike problem illustrated in Figure 2a and 2b but using a power iteration with s = 1. The results are presented in Tables 3 and 4 for gravity and magnetic data, respectively, and they indicate improvements as compared to the results

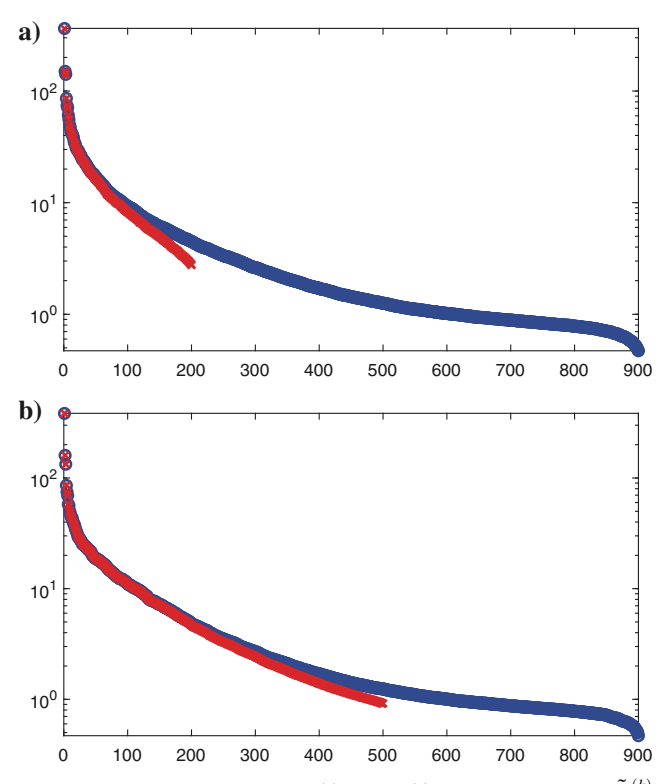


Figure 8. The singular values $\sigma_i^{(k)}$ and $(\sigma_i^{(k)})_q$ for the matrices $\tilde{\tilde{\mathbf{G}}}^{(k)}$ (the blue circles) and $\tilde{\tilde{\mathbf{G}}}_q^{(k)}$ (the red crosses), respectively, for the gravity problem. (a) For q=200 at iteration k=8 and (b) for q=500 at iteration k=8.

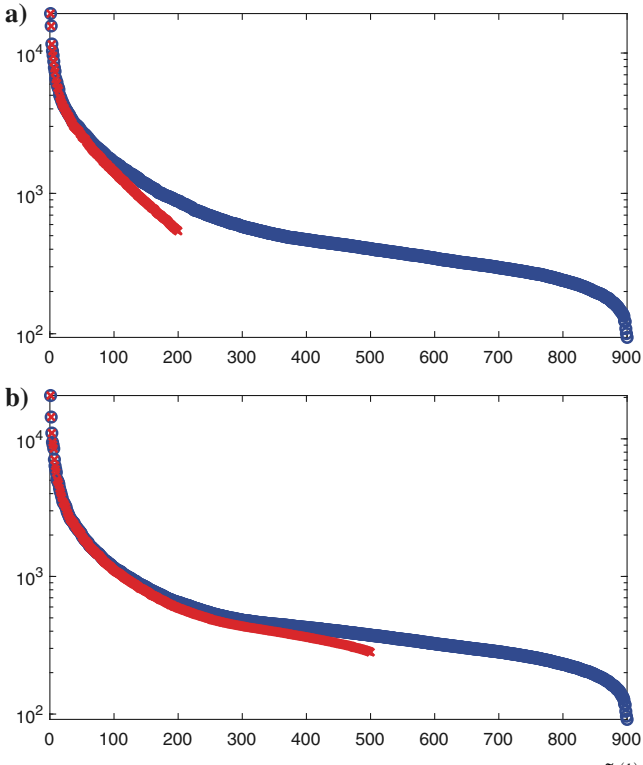


Figure 9. The singular values $\sigma_i^{(k)}$ and $(\sigma_i^{(k)})_q$ for the matrices $\tilde{\tilde{\mathbf{G}}}^{(k)}$ (the blue circles) and $\tilde{\tilde{\mathbf{G}}}_q^{(k)}$ (the red crosses), respectively, for the magnetic problem. (a) For q=200 at iteration k=8 and (b) for q=500 at iteration k=8.

Table 3. Results of the RSVD algorithm via power iterations applied on the gravity data of Figure 2a.

q	$lpha^{(1)}$	$lpha^{(K)}$	$RE^{(K)}$	$RG^{(K)}$	K	χ^2	Time (s)
100	20,629	54.3	0.7018	0.0177	11	913.4	30.4
150	25,862	45.5	0.7288	0.0152	11	909.6	29.5
200	30,218	40.8	0.7185	0.0129	11	904.7	30.9
300	37,279	34.8	0.7188	0.0101	11	898.1	31.8
500	47,447	29.6	0.7099	0.0063	12	851.0	38.0
700	54,892	29.0	0.7093	0.0047	12	893.6	39.6
900	61,712	32.2	0.7232	$1.5534e^{-15}$	12	811.8	41.3

Table 4. Results of the RSVD algorithm via power iterations applied on the magnetic data of Figure 2b.

q	$lpha^{(1)}$	$lpha^{(K)}$	$RE^{(K)}$	$RG^{(K)}$	K	χ^2	Time (s)
100	8375	3127.0	0.9187	0.2880	50	1310.6	128.3
150	9920	3206.5	0.8464	0.2294	50	955.5	128.7
200	11,198	5098.5	0.8235	0.0542	12	915.4	33.2
300	13,235	4447.1	0.8310	0.0323	10	848.9	28.7
500	16,152	3719.6	0.8421	0.0269	9	814.5	29.0
700	18,528	4036.8	0.8405	0.0165	8	887.5	26.7
900	21,086	4106.4	0.8454	$2.0710e^{-15}$	8	898.6	28.7

G102 Vatankhah et al.

presented without power iterations. For both problems, the number of iterations K is generally reduced, once q is large enough, and the error generally is decreased for a result that used the same number of iterations K with and without power iterations. Moreover, the results are achieved without a large increase in computational cost, where the algorithm converged with and without power iterations. But the major impact is that it is possible to take a much smaller q to obtain convergence of the inversion of the magnetic problem with

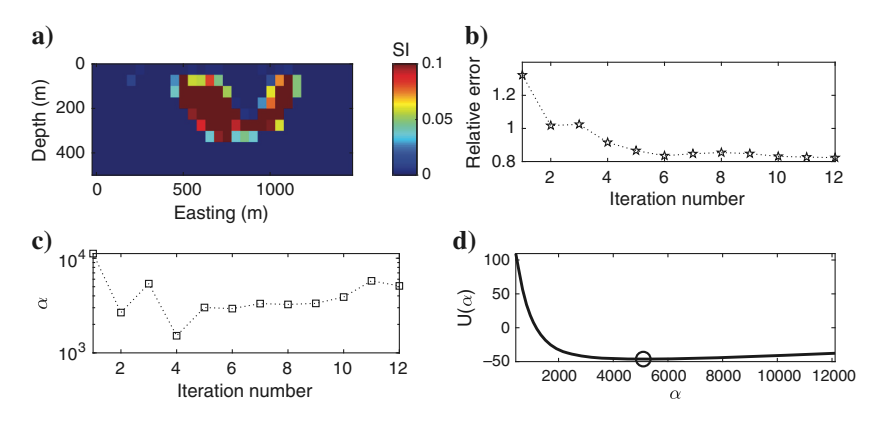


Figure 10. RSVD results using power iterations with s=1 and target rank q=200 for the inversion of magnetic data given in Figure 2b. (a) Cross section of the reconstructed model, (b) the progression of relative error $RE^{(k)}$ with iteration k, (c) the progression of regularization parameter $\alpha^{(k)}$ with iteration k, and (d) the UPRE function at the final iteration.

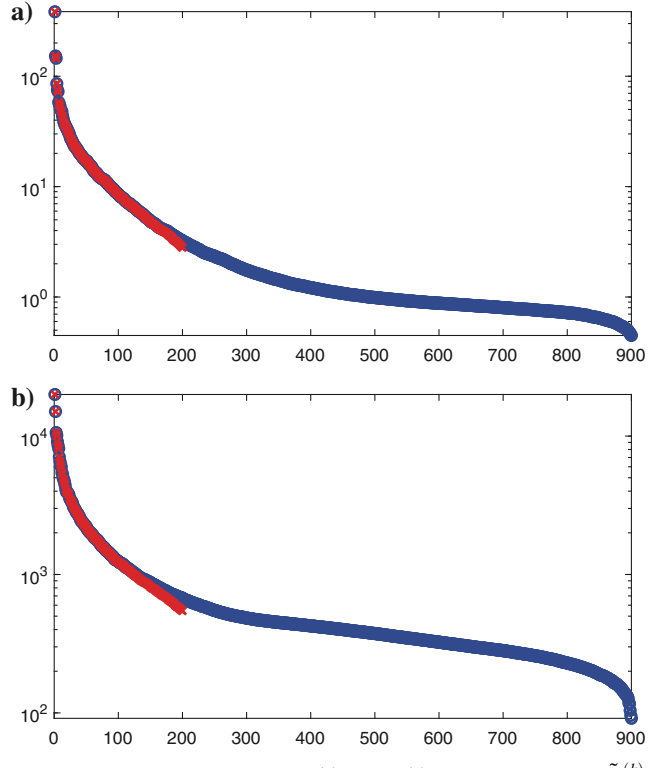


Figure 11. The singular values $\sigma_i^{(k)}$ and $(\sigma_i^{(k)})_q$ for the matrices $\tilde{\tilde{\mathbf{G}}}^{(k)}$ (the blue circles) and $\tilde{\tilde{\mathbf{G}}}_q^{(k)}$ (the red crosses), respectively, for q=200 and s=1. (a) Gravity kernel at iteration k=8 and (b) magnetic kernel at iteration k=8.

reasonable computational cost. In both cases, it is sufficient to now take q=200 to obtain converged solutions for a relatively small K, 11 and 12, respectively.

The results for magnetic data inversion with q = 200 and s = 1 are illustrated in Figure 10 for comparison with Figure 6 obtained without the power iterations. A noticeable improvement in the reconstructed model is obtained. To further show the impact of the power iterations, we also show the singular values for the power

iterations with s=1 and q=200 for the gravity and magnetic problems in Figure 11a and 11b, compared with Figures 8a and 9a, respectively. These plots demonstrate that the power iterations have indeed improved the accuracy of the estimated singular values.

These results naturally raise the question as to whether it is better to apply the RSVD algorithm without power iterations and a large choice for q or to use power iterations and take a smaller q. But the main purpose of using Algorithm 1 is to make it feasible, in terms of memory and computational cost, to find accurate solutions of large-scale problems. Indeed, the aim is to solve problems that are either too expensive to solve using the FSVD or cannot be solved at all using the FSVD; thus, increasing q is not preferred.

Larger problem for a model of multiple bodies

We now study the application of the RSVD algorithm for the solution of a larger and more complex model consisting of six different bodies with different shapes, dimensions, and depths, as shown in the perspective view in Figure 12. The data for the problem are generated on the surface on a 100×80 grid with 100 m spacing. The noisy gravity and magnetic data in each case are illustrated in Figure 13a and 13b.

To perform the inversion, the subsurface volume is discretized into $100 \times 80 \times 10$ cubes of size 100 m in each dimension. The resulting matrix $\tilde{\mathbf{G}}$ is of size 8000×80000 and is too large for efficient use of FSVD. The results obtained using the RSVD algorithm with the choices q = 1000, 1500, 2500, and 4200 are detailed in Tables 5 and 6, respectively, with and without power iterations.

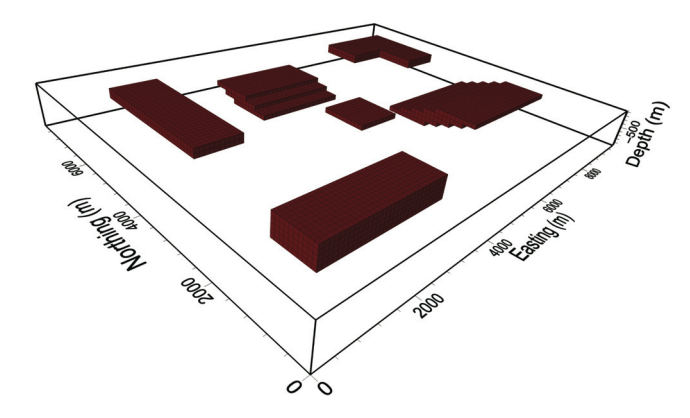


Figure 12. Model consisting of six bodies with different shapes, depths, and dimensions.

As with the inversion of the two-dike problem, it is immediate that the inversions for the gravity problem are acceptable, without power iterations, for far smaller q than for the magnetic case. Applying the power iterations reduces the size of q that is required to obtain convergence, and excellent results are obtained with just q=1000 with a time that is little more than is required for q=1500 and no power iterations. This suggests that we may use $q \gtrsim m/8$ with s=1 for the power iterations. As for the two-dike problem, the magnetic inversion iteration does not converge to the required χ^2 level within 50 iterations, except when we take

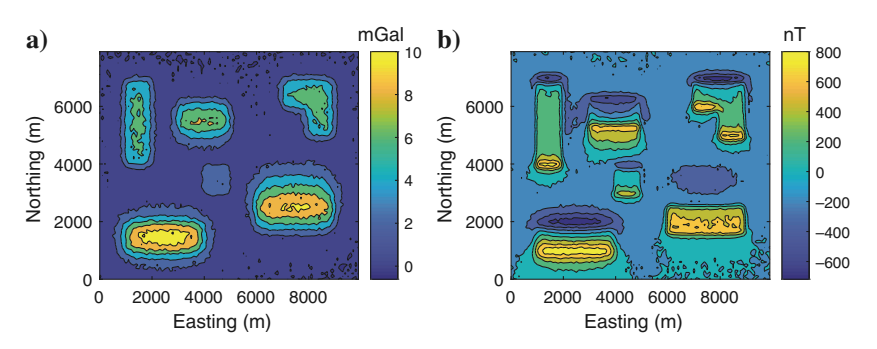


Figure 13. Anomaly produced by the model shown in Figure 12 and contaminated by Gaussian noise. (a) Vertical components of the gravity field. The noise parameters are $(\tau_1 = 0.02, \tau_2 = 0.02)$, (b) total magnetic field. Here, $(\tau_1 = 0.02, \tau_2 = 0.018)$. The S/Ns for the gravity and magnetic data, respectively, are 22.0348 and 21.8817.

q = 4200 > m/2, yielding an error of 1.0975 in approximately 24 min. Including the power iterations yields convergence at K = 14, when q = 2500 with a similar error of 1.0947 after approximately 21 min. These results suggest that it may be acceptable to take $q \gtrsim m/4$ in the inversion of magnetic data with the RSVD algorithm combined with s = 1 power iterations. This choice yields run times for the magnetic inversion that are comparable to those for the gravity inversion.

The perspective views of the reconstructed models using the power iterations and q = 2500 for the gravity and magnetic data

are given in Figures 14 and 15, respectively. The horizontal borders of the reconstructed models, in both inversions, are in good agreement with those of the original model, but additional structures appear at depth. Here, the reconstructed magnetic susceptibility model exhibits more artifacts at depth and has a higher relative error than that achieved for the gravity reconstruction. However, the magnetic structure better illustrates the dip of both dikes, which is significant for accurate geophysical interpretation of the structures. Moreover, these results indicate that joint interpretation of the individual magnetic and gravity inversions may improve the quality of the final subsurface model.

Table 5. Results of the inversion algorithms applied on the gravity data of Figure 13a.

Method	q	$lpha^{(1)}$	$lpha^{(K)}$	$RE^{(K)}$	K	χ^2	Time (s)
RSVD	1000	40,276	38.4	0.7389	21	8108.5	376.8
	1500	48,847	44.6	0.7168	20	7706.2	524.3
	2500	61,439	39.1	0.7111	19	7893.3	946.6
	4200	76,008	37.9	0.7013	20	6943.7	2114.0
RSVD with power iterations	1000	34,324	38.1	0.6927	21	7915.9	617.0
	1500	43,000	36.7	0.6976	20	7985.6	886.3
	2500	56,392	40.0	0.6942	20	7561.5	1775.4
	4200	72,451	38.2	0.6986	20	7989.2	4178.8

Table 6. Results of the inversion algorithms applied on the magnetic data of Figure 13b.

Method	q	$lpha^{(1)}$	$lpha^{(K)}$	$RE^{(K)}$	K	χ^2	Time (s)
RSVD	1000	12,600	10774.9	1.2110	50	26292.4	887.9
	1500	14,564	8947.8	1.1720	50	20789.4	1312.4
	2500	17,376	9253.8	1.1063	50	11891.4	2520.0
	4200	20,695	8778.1	1.0975	13	7750.3	1435.9
RSVD with power iterations	1000	10,705	11128.1	1.1315	50	13480.7	1459.1
	1500	12,744	8992.1	1.0910	50	9570.6	2263.9
	2500	15,837	8425.2	1.0947	14	7863.0	1260.4
	4200	19,518	8665.2	1.1080	12	7299.8	2685.4

G104 Vatankhah et al.

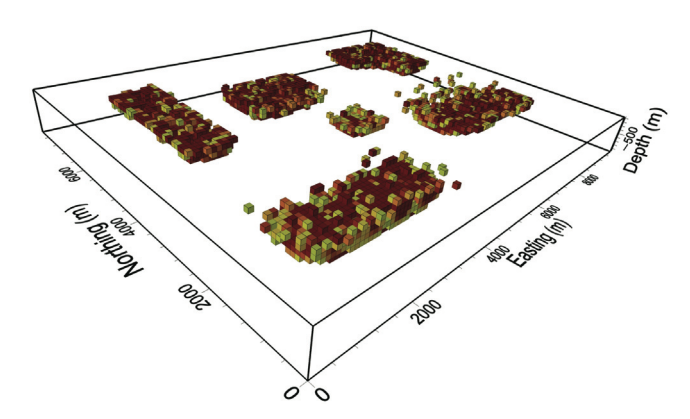


Figure 14. A 3D view of the reconstructed density model, illustrating cells with $\rho > 0.5 \text{ g cm}^{-3}$.

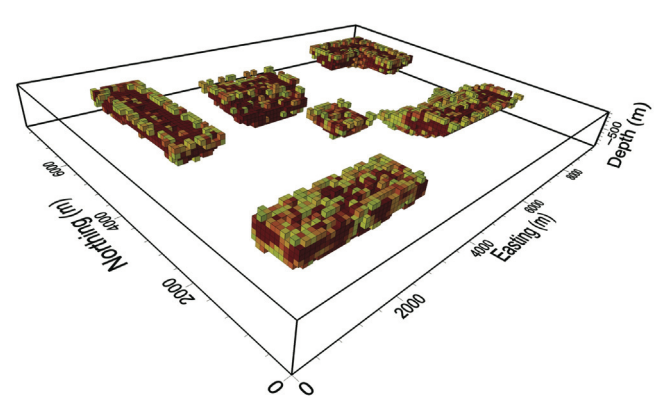


Figure 15. A 3D view of the reconstructed susceptibility model, illustrating cells with $\kappa > 0.05$ (SI unit).

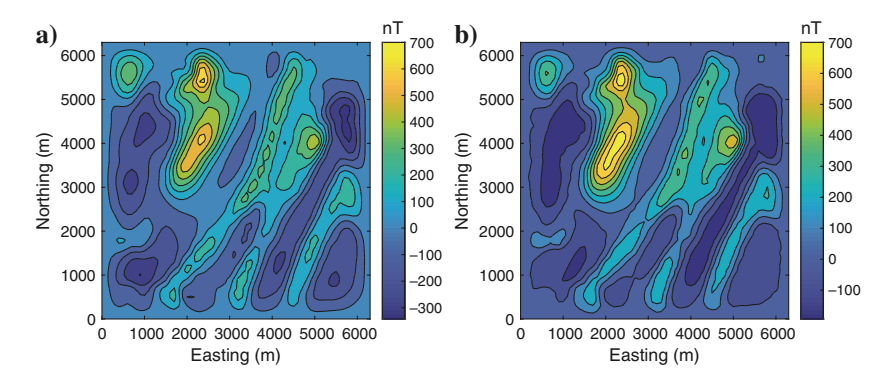


Figure 16. (a) Total magnetic field over a portion of the Wuskwatim Lake region in Manitoba, Canada, and (b) the anomaly produced by the reconstructed model in Figure 17.

REAL DATA

The RSVD algorithm with and without power iterations now is applied for the inversion of total magnetic field data that have been obtained over a portion of the Wuskwatim Lake region in Manitoba, Canada, as shown in Figure 16a. (Results showing the application of the methodology for real gravity data already were presented in Vatankhah et al. [2018b].) The given area lies within a poorly exposed metasedimentary gneiss belt consisting of paragneiss, amphibolite, and migmatite derived from Proterozoic volcanic and sedimentary rocks (Pilkington, 2009). The total field anomaly shows magnetic targets elongated in the northeast-southwest direction. A data-space inversion algorithm with a Cauchy norm sparsity constraint on model parameters was applied by Pilkington (2009) for the inversion of this data set. Furthermore, the results of the inversion algorithm of Li and Oldenburg (1998) also are presented in Pilkington (2009). Therefore, the results presented here can be compared with the results presented in Pilkington (2009), and, for consistency, we thus use a grid of 64×64 data points with 100 m spacing and a uniform subsurface discretization of $64 \times 64 \times 20 =$ 81920 blocks. The intensity of the geomagnetic fields, the inclination, and the declination are 60,000 nT, 78.5°, and 5.3°, respectively. As for the simulations, we set $K_{\text{max}} = 50$, $\mathbf{m}_{\text{apr}} = \mathbf{0}$, and impose bound constraints on the model parameters. In this case, these are 0 = $\kappa_{\min} \le \kappa \le \kappa_{\max} = 0.2$ SI unit (Pilkington, 2009). The values of parameter q are selected based on the recommended choices for the synthetic data examples presented in the previous section. We select q = 1100 > m/4 and q = 2100 > m/2 with and without power iterations, respectively.

The results of the inversions, as given in Table 7, demonstrate that the methodology generates converged solutions using a limited number of iterations and at computational cost on the order of a few minutes only. Overall, these results demonstrate the feasibility of using the RSVD algorithm for the inversion of large-scale geo-

physical data sets. Three plane sections of the reconstructed model obtained using s = 1 for the power iterations are illustrated in Figure 17. The anomaly produced by this model is shown in Figure 16b. The progression of the regularization parameter at each iteration and the UPRE function at the final iteration also are presented in Figure 18. Furthermore, Figure 19 illustrates a 3D view of the model for cells with $\kappa > 0.05$. Our results indicate that, generally, there are three main subsurface targets. The target in the southeast of the area starts from 300 m and extends to 400 m; it is not as deep as the other two targets. The target in the central part of the area is elongated in the southwest-northeast direction, starts from approximately 300 m, and extends to approximately 800 m in depth.

Table 7. Results of the inversion algorithms applied on the magnetic data of Figure 16a.

Method	q	$lpha^{(1)}$	$lpha^{(K)}$	K	χ^2	Time (s)
RSVD	2100	262,575	3630.2	15	4007.1	559.7
RSVD with power iterations	1100	215,644	2906.7	16	4089.7	464.0

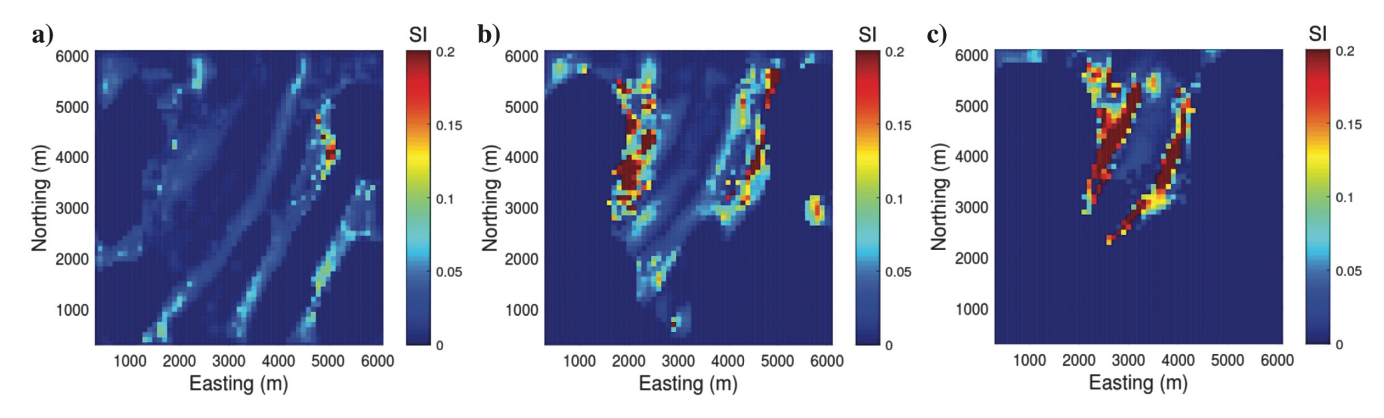


Figure 17. Reconstructed susceptibility model using RSVD via power iterations with s = 1 and target rank q = 1100 for the inversion of magnetic data given in Figure 16a. The plane sections illustrate the depths: (a) 300–400 m, (b) 500–600 m, and (c) 700–800 m.

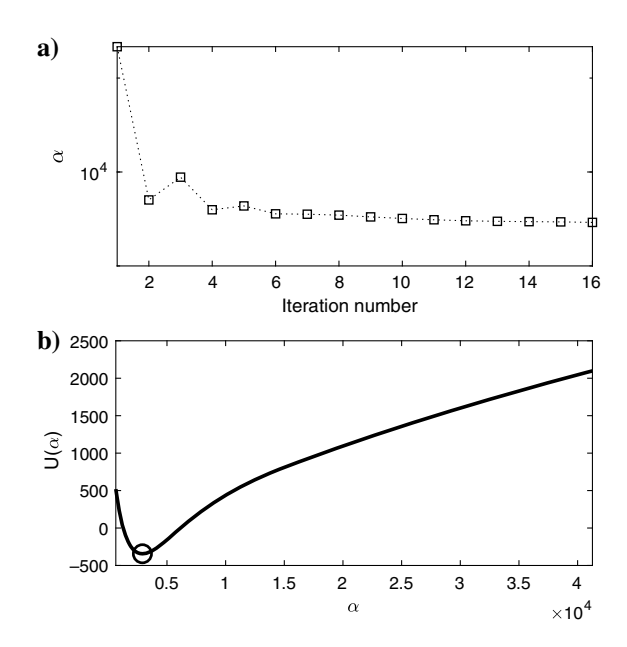


Figure 18. (a) The progression of regularization parameter $\alpha^{(k)}$ with iteration k and (b) the UPRE function at the final iteration.

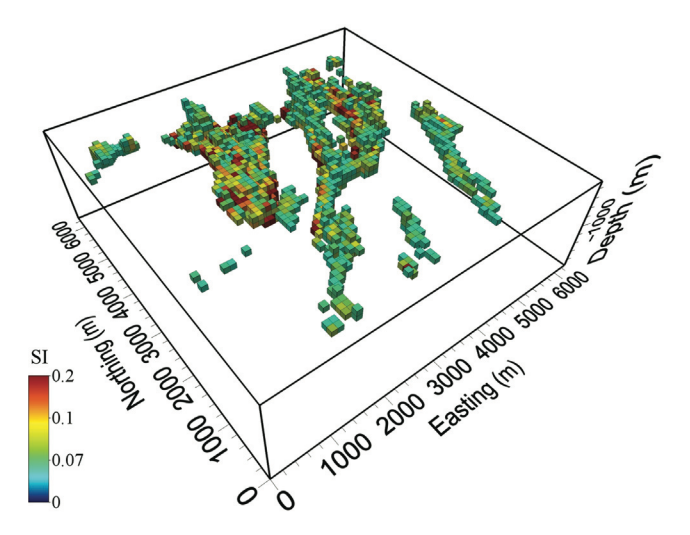


Figure 19. A 3D view of the reconstructed susceptibility model shown in Figure 17, illustrating cells with $\kappa > 0.05$ (SI unit).

This target in its northeastern part is divided into two subparallel targets. The third main target, located in the central north part of the area, is the deepest target, which starts at approximately 400 m and extends to approximately 900 m. The results in the shallow and intermediate layers are in agreement with the results of Pilkington (2009), but at depth, the results presented here are more focused.

CONCLUSION

We present an algorithm for fast implementation of the largescale focusing inversion of magnetic and gravity data, using the memory-demanding sensitivity matrix. The algorithm is based on combining the L_1 -norm regularization strategy for focusing inversion, with RSVD for providing a feasible algorithm for the largescale problem. This demonstrates that the powerful concept of the RSVD provides an attractive and fast alternative to methods such as the GKB algorithm. A comprehensive comparison of the RSVD methodology with power iterations for the inversion of gravity and magnetic data has been presented, and we demonstrated that there is an important difference between gravity and magnetic inverse problems when approximating a q-rank matrix from the original matrix. For the inversion of magnetic data, it is necessary to take larger values of q, compared with the inversion of gravity data, in order that a suitable approximation of the sensitivity matrix is obtained. Furthermore, including power iterations within the algorithm improves the approximation quality. Indeed, the RSVD obtained using the power iterations step yields a good approximation of the dominant singular space for small choices of q, yielding an efficient strategy when the singular values of the input matrix decay slowly. Thus, with just one power iteration for each input matrix, acceptable results are achieved via $q \gtrsim m/4$ and $q \gtrsim m/8$ for magnetic and gravity inversion, respectively. The presented methodology can be used for other geophysical data sets, and the choice of the rank q approximation will depend on the spectral properties of the relevant kernel matrices. If the RSVD without power iteration does not approximate the dominant singular values for low-rank approximations, then power iterations should be included to improve the quality of the estimated singular values. The simulations, and results for real data, demonstrate that the algorithm is effective for sensitivity matrices requiring storage of at least 640 million entries, and solutions are obtained on a desktop computer within approximately 30 min. Furthermore, our results show that the regularization parameters used, and automatically estimated in the inversion algorithm, are much larger for the inversion of the magnetic data. This also is a reflection of the different spectral properties of the magnetic and gravity input matrices. In conclusion, we have demonstrated that it is feasible to use an efficient, in computational time and memory, RSVD methodology for problems that are too large to be handled using the full SVD.

We note, furthermore, that when it is not possible to transfer the global objective function into the standard form, the presented RSVD algorithm is not practical. For example, for inversion using a total variation regularization, it still is possible to use an iteratively reweighted algorithm but now applied with the calculation of the generalized SVD at each iteration. This also is computationally demanding; hence, techniques using the generalized randomized SVD can be used. Further development of that approach is needed to make an algorithm that is feasible for use with sensitivity matrices of the sizes considered here.

ACKNOWLEDGMENTS

The authors would like to thank M. Pilkington for providing data from the Wuskwatim Lake area. We also are very appreciative of the suggestions made by the associate editor Y. Li, reviewer V. C. F. Barbosa, and two anonymous reviewers. Their comments assisted significantly with the presentation of the contributions of the paper. This study was financially supported by the National Key R&D Program of China (grant nos. 2016YFC0600109 and 2017YFC0602405) and the China Postdoctoral Science Foundation (grant no. 2019M660191). R. Renaut acknowledges the support of NSF grant DMS 1913136: Approximate Singular Value Expansions and Solutions of Ill-Posed Problems.

DATA AND MATERIALS AVAILABILITY

Data associated with this research are confidential and cannot be released.

REFERENCES

- Blakely, R. J., 1996, Potential theory in gravity & magnetic applications, Cambridge University Press.
- Boulanger, O., and M. Chouteau, 2001, Constraints in 3D gravity inversion: Geophysical Prospecting, 49, 265–280, doi: 10.1046/j.1365-2478.2001.00254.x.
- Chung, J., J. Nagy, and D. P. O'Leary, 2008, A weighted GCV method for Lanczos hybrid regularization: Electronic Transactions on Numerical Analysis, 28, 149–167.
- Chung, J., and K. Palmer, 2015, A hybrid LSMR algorithm for large-scale Tikhonov regularization: SIAM Journal on Scientific Computing, 37, S562–S580, doi: 10.1137/140975024.
- Cox, H. L., G. A. Wilson, and M. S. Zhdanov, 2010, 3D inversion of air-borne electromagnetic data using a moving footprint: Exploration Geophysics, 41, 250–259, doi: 10.1071/EG10003.
- Erichson, N. B., S. Voronin, and S. L. Brunton, 2016, Randomized matrix decompositions using R, arXiv preprint, arXiv:1608.02148, https://arxiv.org/abs/1608.02148.
- Farquharson, C. G., 2008, Constructing piecewise-constant models in multidimensional minimum-structure inversions: Geophysics, 73, no. 1, K1– K9, doi: 10.1190/1.2816650.
- Farquharson, C. G., and D. W. Oldenburg, 2004, A comparison of automatic techniques for estimating the regularization parameter in non-linear inverse problems: Geophysical Journal International, 156, 411–425, doi: 10.1111/j.1365-246X.2004.02190.x.
- Golub, G. H., and C. F. Van Loan, 2013, Matrix computations, 4th ed.: John Hopkins University Press.
- Haáz, I. B., 1953, Relations between the potential of the attraction of the mass contained in a finite rectangular prism and its first and second derivatives: Geofizikai Kozlemenyek, 2, 57–66.

- Halko, N., P. G. Martinsson, and J. A. Tropp, 2011, Finding structure with randomness: Probabilistic algorithms for constructing approximate matrix decompositions: SIAM Review, 53, 217–288, doi: 10.1137/090771806.
- Kilmer, M. E., and D. P. O'Leary, 2001, Choosing regularization parameters in iterative methods for ill-posed problems: SIAM Journal on Matrix Analysis and Applications, 22, 1204–1221, doi: 10.1137/S0895479899345960
- Lelièvre, P. G., and D. W. Oldenburg, 2006, Magnetic forward modelling and inversion for high susceptibility: Geophysical Journal International, **166**, 76–90, doi: 10.1111/j.1365-246X.2006.02964.x.
- Li, Y., and D. W. Oldenburg, 1996, 3-D inversion of magnetic data: Geophysics, 61, 394–408, doi: 10.1190/1.1443968.
- Li, Y, and D. W. Oldenburg, 1998, 3-D inversion of gravity data: Geophysics, **63**, 109–119, doi: 10.1190/1.1444302.
- Li, Y., and D. W. Oldenburg, 2003, Fast inversion of large-scale magnetic data using wavelet transforms and a logarithmic barrier method: Geophysical Journal International, 152, 251–265, doi: 10.1046/j.1365-246X .2003.01766.x.
- Liu, S., M. Fedi, X. Hu, Y. Ou, J. Baniamerian, B. Zuo, Y. Liu, and R. Zhu, 2018, Three-dimensional inversion of magnetic data in the simultaneous presence of significant remanent magnetization and self-demagnetization: Example from Daye iron-ore deposit, Hubei province: Geophysical Journal International, 215, 614–634, doi: 10.1093/gji/ggy299.
 Liu, S., X. Hu, T. Liu, J. Feng, W. Gao, and L. Qiu, 2013, Magnetization
- Liu, S., X. Hu, T. Liu, J. Feng, W. Gao, and L. Qiu, 2013, Magnetization vector imaging for borehole magnetic data based on magnitude magnetic anomaly: Geophysics, 78, no. 6, D429–D444, doi: 10.1190/geo2012-0454.1.
- Martinsson, P. G., 2016, Randomized methods for matrix computations and analysis of high dimensional data, arXiv preprint, arXiv:1607.01649, https://arxiv.org/abs/1607.01649.
- Nabighian, M. N., M. E. Ander, V. J. S. Grauch, R. O. Hansen, T. R. Lafehr, Y. Li, W. C. Pearson, J. W. Peirce, J. D. Philips, and M. E. Ruder, 2005, Historical development of the gravity method in exploration: Geophysics, 70, no. 6, 63ND–89ND, doi: 10.1190/1.2133785.
- Oldenburg, D. W., P. R. McGillivray, and R. G. Ellis, 1993, Generalized subspace methods for large-scale inverse problem: Geophysical Journal International, **114**, 12–20, doi: 10.1111/j.1365-246X.1993.tb01462.x.
- Paige, C. C., and M. A. Saunders, 1982a, LSQR: An algorithm for sparse linear equations and sparse least squares: ACM Transactions on Mathematical Software, 8, 43–71, doi: 10.1145/355984.355989.
- Paige, C. C., and M. A. Saunders, 1982b, ALGORITHM 583 LSQR: Sparse linear equations and least squares problems: Transactions on Mathematical Software, **8**, 195–209, doi: 10.1145/355993.356000.
- Paoletti, V., P. C. Hansen, M. F. Hansen, and M. Fedi, 2014, A computationally efficient tool for assessing the depth resolution in potential-field inversion: Geophysics, 79, no. 4, A33–A38, doi: 10.1190/geo2014-0017.1.
- inversion: Geophysics, **79**, no. 4, A33–A38, doi: 10.1190/geo2014-0017.1. Pilkington, M., 1997, 3-D magnetic imaging using conjugate gradients: Geophysics, **62**, 1132–1142, doi: 10.1190/1.1444214.
- Pilkington, M., 2009, 3D magnetic data-space inversion with sparseness constraints. Geophysics 74, no. 1, 17-115, doi: 10.1190/1.3026538
- constraints: Geophysics, **74**, no. 1, L7–L15, doi: 10.1190/1.3026538. Portniaguine, O., and M. S. Zhdanov, 1999, Focusing geophysical inversion images: Geophysics, **64**, 874–887, doi: 10.1190/1.1444596.
- Portniaguine, O., and M. S. Zhdanov, 2002, 3D magnetic inversion with data compression and image focusing: Geophysics, 67, 1532–1541, doi: 10 1190/1 1512749
- Rao, D. B., and N. R. Babu, 1991, A rapid method for three-dimensional modeling of magnetic anomalies: Geophysics, 56, 1729–1737, doi: 10 .1190/1.1442985.
- Renaut, R. A., S. Vatankhah, and V. E. Ardestani, 2017, Hybrid and iteratively reweighted regularization by unbiased predictive risk and weighted GCV for projected systems: SIAM Journal on Scientific Computing, 39, no. 2, B221–B243, doi: 10.1137/15M1037925.
- Silva, J. B. C., and V. C. F. Barbosa, 2006, Interactive gravity inversion: Geophysics, 71, no. 1, J1–J9, doi: 10.1190/1.2168010.

 Skilling, J., and R. K. Bryan, 1984, Maximum entropy image reconstruction:
- Skilling, J., and R. K. Bryan, 1984, Maximum entropy image reconstruction: General algorithm: Monthly Notices of the Royal Astronomical Society, 211, 111–124, doi: 10.1093/mnras/211.1.111.
- 211, 111–124, doi: 10.1093/mnras/211.1.111.

 Uieda, L., and V. C. F. Barbosa 2012, Robust 3D gravity gradient inversion by planting anomalous densities: Geophysics, 77, no. 4, G55–G66, doi: 10.1190/geo2011-0388.1.
- Vatankhah, S., V. E. Ardestani, and R. A. Renaut, 2015, Application of the χ^2 principle and unbiased predictive risk estimator for determining the regularization parameter in 3D focusing gravity inversion: Geophysical Journal International, **200**, 265–277, doi: 10.1093/gji/ggu397.
- Vatankhah, S., R. A. Renaut, and V. E. Ardestani, 2017, 3-D projected L_1 inversion of gravity data using truncated unbiased predictive risk estimator for regularization parameter estimation: Geophysical Journal International, 210, 1872–1887, doi: 10.1093/gji/ggx274.
- Vatankhah, S., R. A. Renaut, and V. E. Ardestani, 2018a, Total variation regularization of the 3-D gravity inverse problem using a randomized generalized singular value decomposition: Geophysical Journal International, 213, 695–705, doi: 10.1093/gji/ggy014.

- Vatankhah, S., R. A. Renaut, and V. E. Ardestani, 2018b, A fast algorithm for regularized focused 3D inversion of gravity data using the randomized singular-value decomposition: Geophysics, **83**, no. 4, G25–G34, doi: 10
- Singular-value decomposition. Geophysics, 83, no. 4, 023–034, doi: 10.1190/geo2017-0386.1.
 Vatankhah, S., R. A. Renaut, and S. Liu, 2020, Research note: A unifying framework for the widely used stabilization of potential field inverse problems: Geophysical Prospecting, 68, 1416–1421, doi: 10.1111/1365-2478.12026
- Vogel, C. R., 2002, Computational methods for inverse problems, SIAM Frontiers in Applied Mathematics: SIAM.
 Voronin, S., D. Mikesell, and G. Nolet, 2015, Compression approaches
- for the regularized solutions of linear systems from large-scale inverse
- problems: International Journal on Geomathematics, 6, 251-294, doi:
- Wei, Y., P. Xie, and L. Zhang, 2016, Tikhonov regularization and randomized GSVD: SIAM Journal on Matrix Analysis and Application, 37, 649–675, doi: 10.1137/15M1030200.
- 649–67s, doi: 10.1137/15M1030200.

 Xiang, H., and J. Zou, 2013, Regularization with randomized SVD for large-scale discrete inverse problems: Inverse Problems, 29, 085008, doi: 10.1088/0266-5611/29/8/085008.

 Xiang, H., and J. Zou, 2015, Randomized algorithms for large-scale inverse problems with general Tikhonov regularization: Inverse Problems, 31, 085008, doi: 10.1088/0266-5611/31/8/085008.